
APR Turbulence and Diffusion Note No. 273

# Idealised simulations of mountain forced gravity waves using the 2D New Dynamics

by

Samantha Smith
Adrian Broad

21st May 2001

Met Office
London Road
Bracknell
Berkshire, RG12 2SZ

© Crown Copyright 2001

This paper has not been published. Permission to quote from it should be obtained from the Head of Atmospheric Processes Research, Met Office.

DU... ...ALSO

NATIONAL METEOROLOGICAL LIBRARY

# Idealised Simulations of Mountain Forced Gravity Waves using the 2-D New Dynamics

Samantha Smith and Adrian Broad

## 1 Introduction

The 2D New Dynamics model is a vertical slice version of the 3D New Dynamics, which solves the fully compressible, inviscid, non-hydrostatic equations of motion. It uses a semi-Lagrangian horizontal advection scheme and a semi-implicit time-stepping adjustment scheme. The Charney Phillips vertical grid is employed with a hybrid height vertical coordinate. Model levels are terrain-following near the surface and constant height at the top, varying smoothly between the two at intermediate levels. Moisture is not included, although the inclusion of moist air is possible.

This report describes idealised high resolution simulations of stable airflow over small mountains. Initial test simulations of vertically propagating gravity waves reveal that wave reflections seriously contaminate the wave-field due to the use of a rigid lid at the upper boundary. The effectiveness of using sponge layers in reducing these reflections is tested, and sensitivity tests are carried out on resolution, time-step and domain size.

## 2 Sponge Tests for Hydrostatic Gravity Waves

### 2.1 Initial Conditions

The flow of air with constant upstream Brunt-Vaisala frequency N equal to 0.01 $s^{-1}$ and constant wind-speed U equal to 10 m $s^{-1}$ over a small mountain was simulated using a Witch of Agnesi mountain profile of the form

$$h(x) = \frac{h_0 a^2}{a^2 + (x - x_0)^2}$$

where $h_0$ is the peak mountain height and a is the half-width of the mountain, given values of 50m and 5km respectively. The position of the centre of the mountain is given by $x_0$. The resulting slope is gentle, and the flow is expected to be linear, with a non-dimensional mountain height (Nh/U) of 0.05. Also, the non-dimensional mountain width (Na/U) was 5, leading to a hydrostatic gravity wave field. The mountain was placed at the centre of the domain, as hydrostatic waves propagate vertically immediately above the mountain.

These initial tests were carried out using a fairly small domain to reduce the required computer time. The domain chosen was 100km long and 30km high. This domain is long enough so that the local mountain height falls to zero at the lateral boundaries (although this is actually specified as zero within the initialisation code), and tall enough to allow a sufficiently deep gravity wave field to develop

before reaching the top boundary. An initial horizontal grid spacing (dx) of 500m was chosen to ensure high enough horizontal resolution to capture the expected wave activity. For a mountain of half-width 5km, giving a mountain which is about 20km wide, a 500m grid spacing results in 40 grid-points over the mountain, so that any motions resulting from flow over the mountain will be resolved in the horizontal. An initial vertical grid spacing (dz) of 750m was chosen (40 vertical levels). The expected vertical wavelength of the hydrostatic gravity wave $\lambda_z$, given by $2\pi$U/N, is approximately 6km, so a vertical grid spacing of 750m results in 8 grid-points per wave, which should be sufficient to resolve it (Klemp and Lilly, 1978). A constant vertical grid was used to keep the resolution high in the upper model levels. Inflow/outflow lateral boundary conditions were chosen rather than periodic ones so as not to contaminate the incoming wind field.

The Courant number (CFL = U dt/dx) for these runs was chosen as 1, resulting in a time-step (dt) of 50s. With a mean wind-speed of 10 m $s^{-1}$, the flow crosses the model domain in 10000 seconds (200 timesteps). The mountain was grown slowly over this initial 10000 seconds and the model was run for an extra 10000 seconds after this to enable the wave field to develop fully.

Figure (1a) shows the resulting vertical velocity field (W) at the end of this simulation. The contour spacing is 0.04 m $s^{-1}$. Due to the decreasing density with height, the hydrostatic gravity wave amplifies with height. In the real atmosphere, these waves would continue to propagate vertically until they reach instability due to their large amplitude or they reach a critical level where they break and dissipate. However, the simulated waves are reflected by the rigid lid, and the detrimental effect on the wave field is clearly seen.

## 2.2 The Effect of using a Sponge Layer

After each time-step (n $\times$ dt, where n is an integer) a parameter such as U will change from $U_{n-1}$ to $U_n$ by the addition of an incremental change. To prevent reflections from the rigid lid, motions are damped out in the upper part of the domain using a sponge layer starting from a specified height $z_{base}$. The damping increases with height within the sponge layer from nothing at $z_{base}$ to a maximum at the top of the domain $z_{top}$. This is achieved by applying a weighting function to the data-fields within the sponge layer. The strongest sponge function available in the 2D code was chosen, the cosine squared sponge function, defined as

$$W = \alpha + (1 - \alpha)Cos^2(\frac{\pi}{2}\frac{(z-z_{base})}{(z_{top}-z_{base})})$$

The strength of the sponge is defined by the value of the parameter $\alpha$, which can have any value between 1 and 0, with 0 giving the strongest damping. The value of U within the sponge layer, $U_{sponge}$ then becomes

$$U_{sponge} = WU_n + (1 - W)U_{n-1}$$

At the top edge of the domain, only a small fraction of the incremented value is added onto the field, thereby blending the data field back into the initial field.

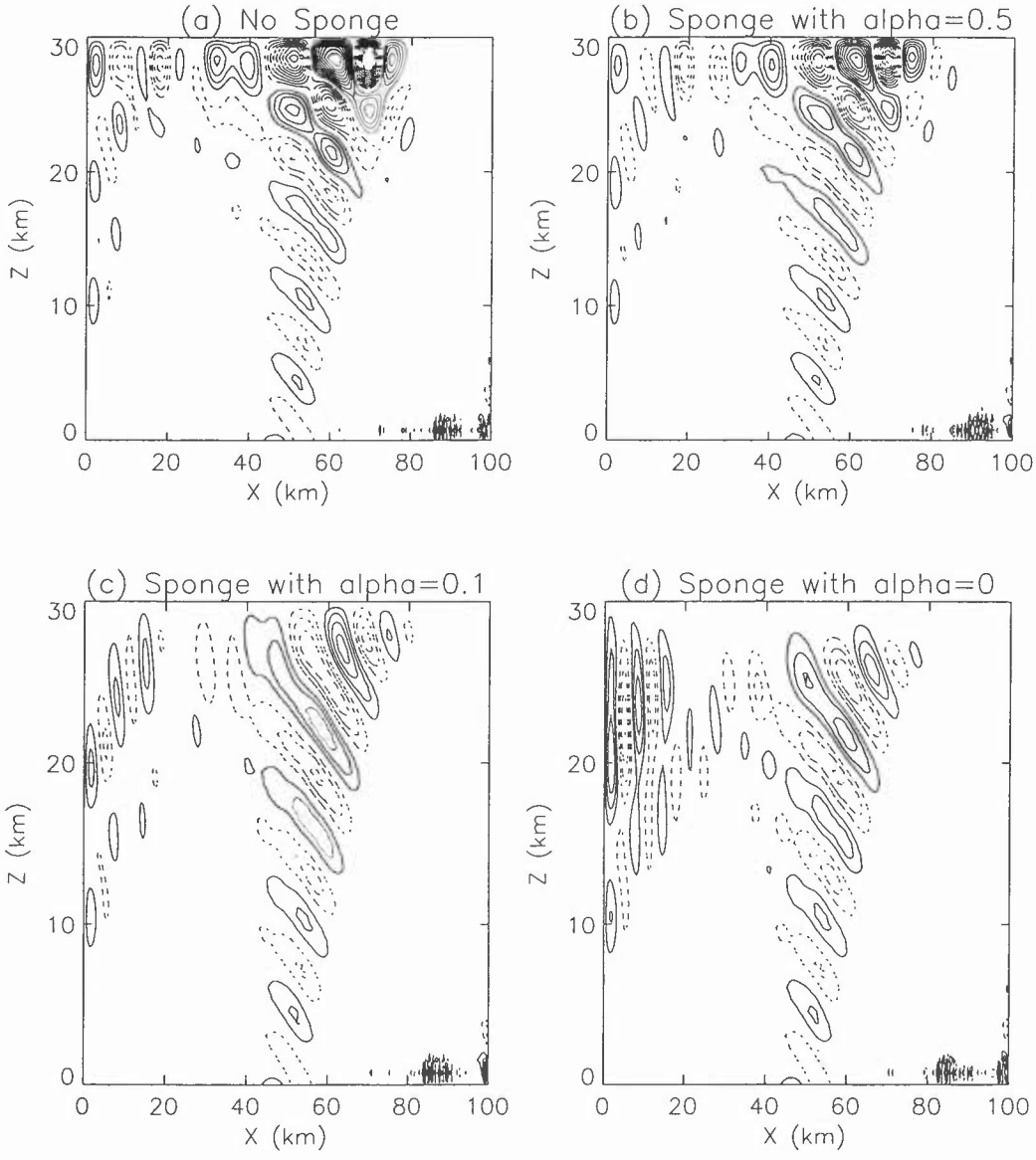


Figure 1: Hydrostatic vertically propagating gravity waves: Vertical velocity field after 20,000s simulation with sponge layers at the top of the domain of different strengths. The contour spacing is 0.04 m $s^{-1}$

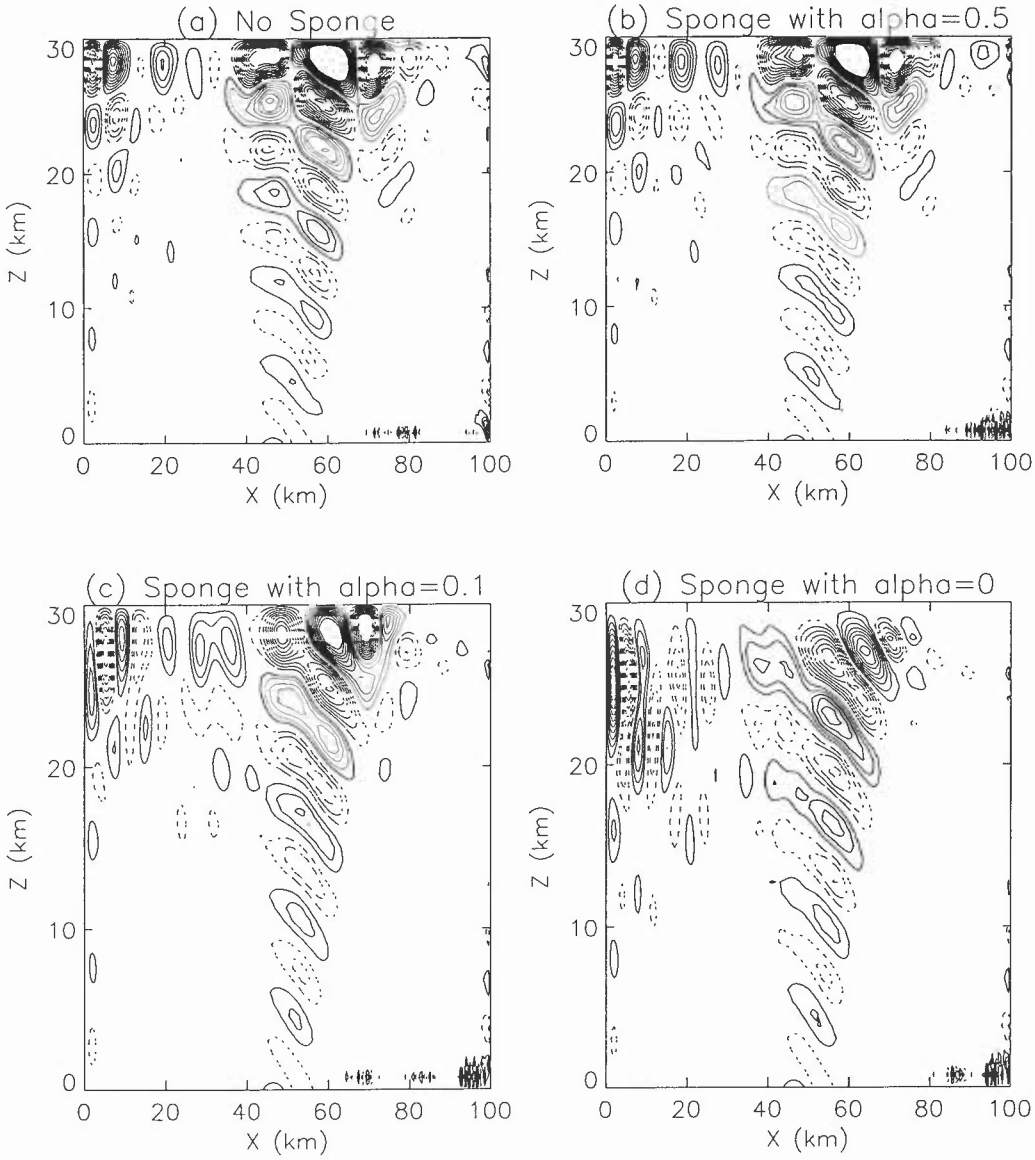


Figure 2: As for figure (1) but after 40,000s simulation.

Figure (1b) to (1d) shows the effect of applying a 15km deep sponge layer of various strengths on the vertical velocity field for the simulation described in the previous section. Again, the contour spacing is 0.04 m $s^{-1}$.

The strength is increased in successive simulations by decreasing the value of $\alpha$, using 0.5 (figure 1b), 0.1 (figure 1c) and 0 (figure 1d). For $\alpha$ equal to zero, the weighting function described above reduces to

$$W = Cos^2\left(\frac{\pi}{2}\frac{(z-z_{base})}{(z_{top}-z_{base})}\right)$$

and the value of U at the highest model level should remain at the initial value of 10 m $s^{-1}$. As this is the strongest sponge, wave reflections from the rigid lid are considerably reduced, as can be seen in the diagram, by limiting the amount of wave energy reaching the top of the domain. Table (1) lists the maximum positive and negative vertical velocity magnitudes for each figure over the entire model domain and in the lowest 10km. The maximum vertical velocity magnitude, which is found near the top of the model domain, was reduced by the strongest sponge layer from 0.42 m $s^{-1}$ in the control run to below 0.16 m $s^{-1}$, a reduction by a factor of 2.6. Meanwhile, the wave magnitude below 10km (the tropopause height in the real atmosphere) has remained essentially unchanged at approximately 0.088 m $s^{-1}$. However, there is a lot of noise present on the left hand side of the domain, more so even than for the original run and is therefore possibly due to the sponge layer itself. This will be dealt with later using lateral sponge layers. There is also some spurious very small scale noise in the lowest layer still, due possibly to numerical instability, or an isentropic lower boundary problem.

Figures (2) show the results of running the above simulations for a further 20000 seconds, taking the total run time up to 40000 seconds. It is obvious that running the simulation for longer than the original 20000 seconds is detrimental to the wave field as it has already reached the top of the domain. The maximum vertical velocity magnitude near the top of the domain increases by between 50 and 100% during this time (see table 1).

## 2.3 The Effect of Varying the Sponge Layer Depth

The depth over which the sponge layer is applied is also an important consideration. Klemp and Lilly (1978) suggested that the absorption layer depth must be larger than the vertical wavelength ($\lambda_z$) in order for it to be able to properly damp out the wave response towards the domain top. The hydrostatic wavelength was approximately 6 km for this case, and thus a 15km deep sponge contains more than 2 vertical wavelengths.

The effect of varying the depth of the sponge layer, D, is shown in Figure 2. Parts (a,b and c) show the vertical velocity field with the sponge layer depth specified as 10 km, 15 km and 20 km, respectively. A deeper sponge layer results in more of the wave field being damped out in the upper part of the domain because the sponge starts to work lower down. This can also be seen in the velocity magnitudes in table 1. However, the sponge layer should ideally be optimised to give the largest damping in the upper levels while not affecting the region of interest in each specific experiment. For subsequent tests, the sponge depth is kept at 15km as a compromise.

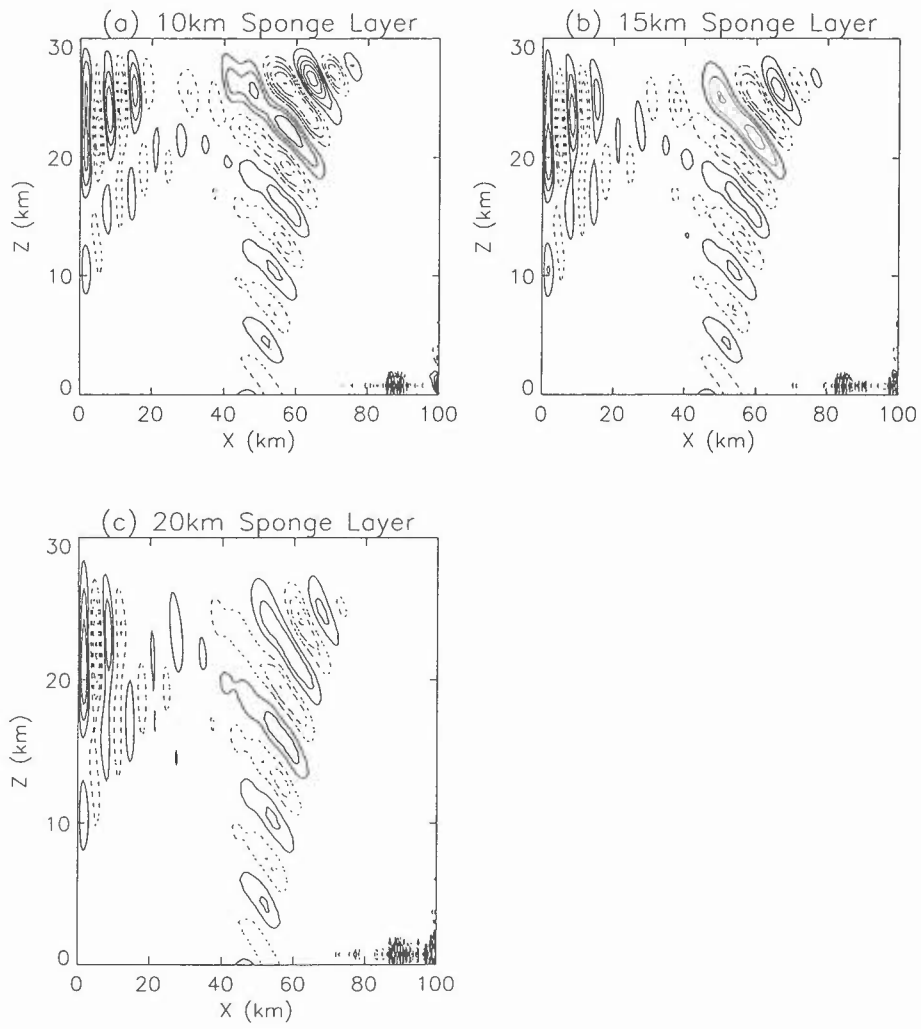


Figure 3: Vertical velocity field after 20,000s simulation: Effect of varying the sponge layer depth. The contour spacing is 0.04 m $s^{-1}$

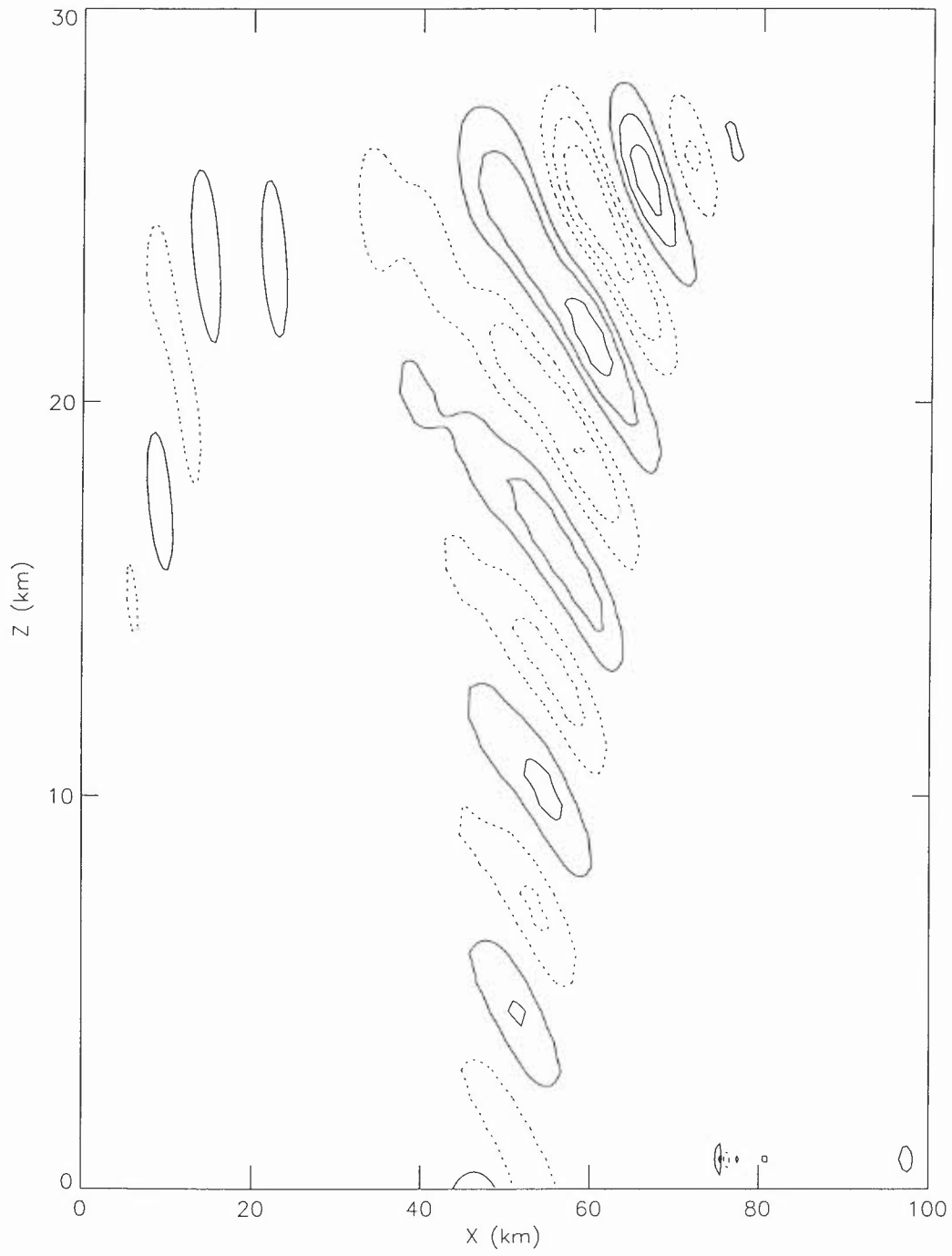


Figure 4: Vertical velocity field after 20,000s simulation, with a 15km deep sponge layer at the top of the domain and lateral sponges of width 20km. The contour spacing is 0.04 m $s^{-1}$

## 2.4 The Effect of Adding Lateral Sponge Layers

The results in the previous sections show that a sponge layer can successfully damp many of the reflections from the rigid lid, as long as the simulation is not run for too long.

Lateral sponge layers with the same cosine squared sponge function were applied to both inflow and outflow boundaries with $\alpha$ equal to zero. The width of each lateral sponge layer was specified as 20km so as not to affect the actual wave field. With a horizontal resolution of 500m, each sponge layer covers 40 grid-points. The resulting vertical velocity field at the end of a 20000 second simulation is shown in figure (3) with contour interval 0.04 m $s^{-1}$. There is again a large improvement in the results, but it is still not perfect. The following few sections describe the results of simulations at different resolutions, using different time-steps and for larger domains, using the same initial atmospheric profile and mountain shape as described above and the same sponge layers as used in this section.

## 2.5 The Effect of Changing the Vertical Resolution

The above simulation was carried out again but using different vertical grids. Figure (4) shows the vertical velocity field resulting from a 20000 second simulation using (a) a constant vertical grid with a resolution of 750m as before, (b) a constant vertical grid with a resolution of 500m, and (c) a constant vertical grid with a resolution of 375m. This time the contour interval has been reduced to 0.025 m $s^{-1}$ to better show the wave field itself now that much of the noise has been eliminated. Increasing the vertical resolution from 750m to 500m improves the resultant wave field by increasing the accuracy of the model. The contours are much smoother and the very small scale numerical noise in the lowest layer has disappeared. The number of vertical grid-points per wave has been increased from 8 to 12. Increasing the vertical resolution again to 375m (16 grid-points per wave) improves the wave field again but the improvement is much smaller, indicating that the model is tending towards the correct solution. Figure (5) shows the linear analytical solution for these conditions as in Smith (1979), with 0.025 m $s^{-1}$ contour spacing. The maximum values of u and w over both the entire domain and within the lowest 10km are given. The model solution should be compared to the linear analytical solution in the lower levels as the wave field there is uncontaminated by reflections from the lid and it corresponds to the troposphere in the real atmosphere.

The model does very well at reproducing the linear analytical wave-field in the lowest 10km when the vertical resolution is improved to 500m or better. The contours here look similar to the linear solution in figure 5. A better comparison is made by examining the wave magnitudes in the lowest 10km of the domain as given in table 1. The wave magnitudes for the original layer spacing of 750m were actually too small by greater than 10%. However, the wave magnitudes for the simulations with smaller grid spacing differ from the linear solution values by only 5% or less.

## 2.6 The Effect of Changing the Time-step

The simulation was repeated using a vertical resolution of 375m and a horizontal resolution of 500m, while the time-step was varied between 12.5 and 100 seconds as shown in figure (6), with contour interval 0.025 m $s^{-1}$. This changes the Courant number between 0.25 and 2. The mountain was grown over 10000 seconds in all cases.

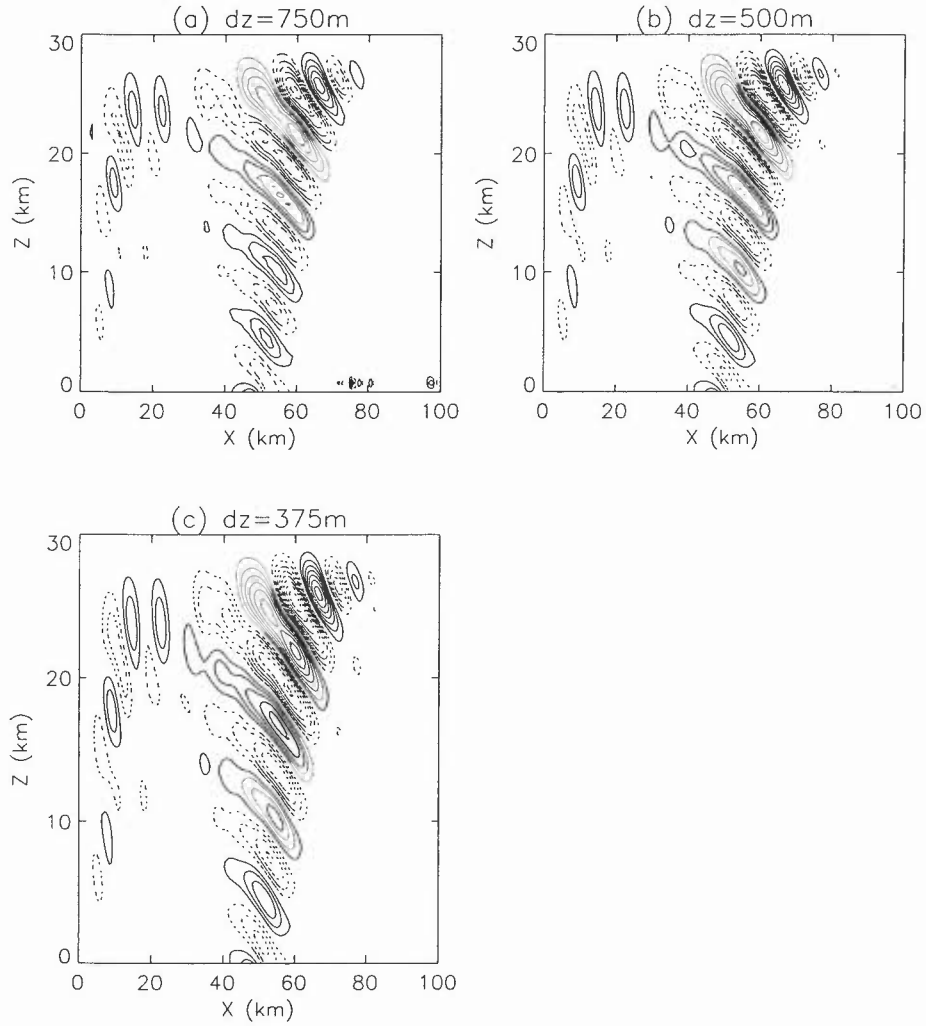


Figure 5: Vertical velocity field after 20,000s simulation: Effect of varying the vertical resolution. The contour spacing is 0.025 m $s^{-1}$

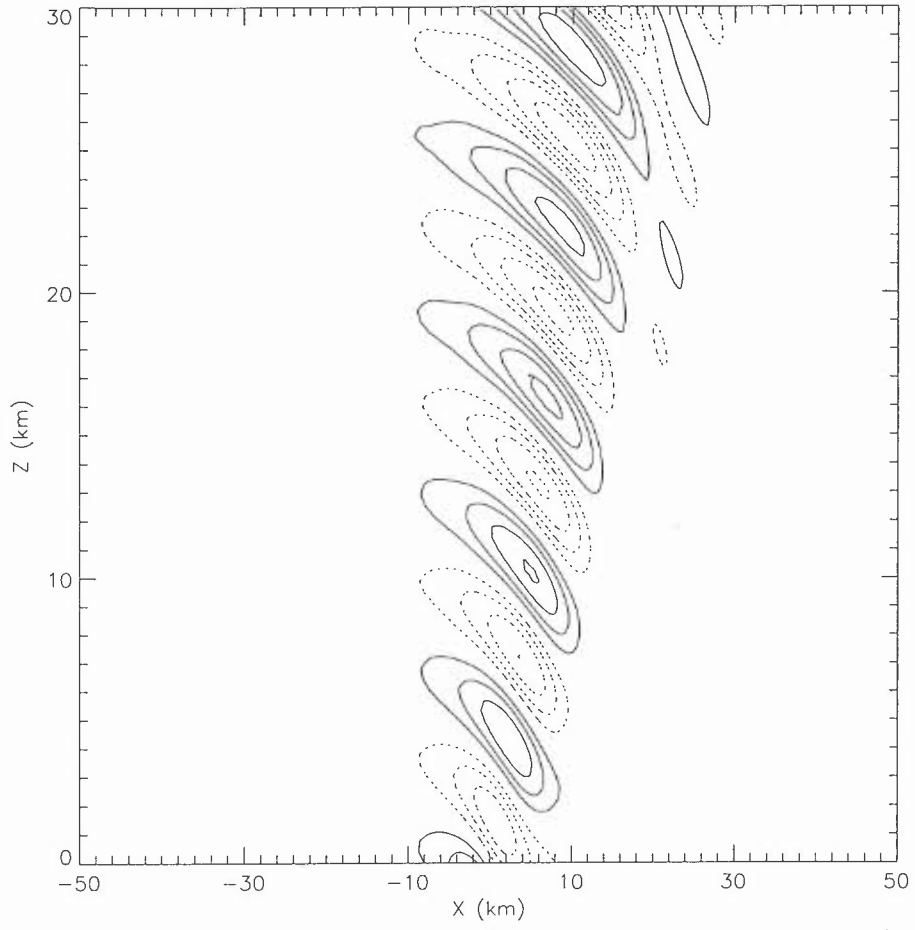


Low Level Range

Max W = 0.118600

Max W = −0.101368, 0.101628

Max U = 0.585823

Max U = −0.434373, 0.453397

Max Psurf = 0.480752

Figure 6: Linear analytical solution. The contour spacing is 0.025 m $s^{-1}$

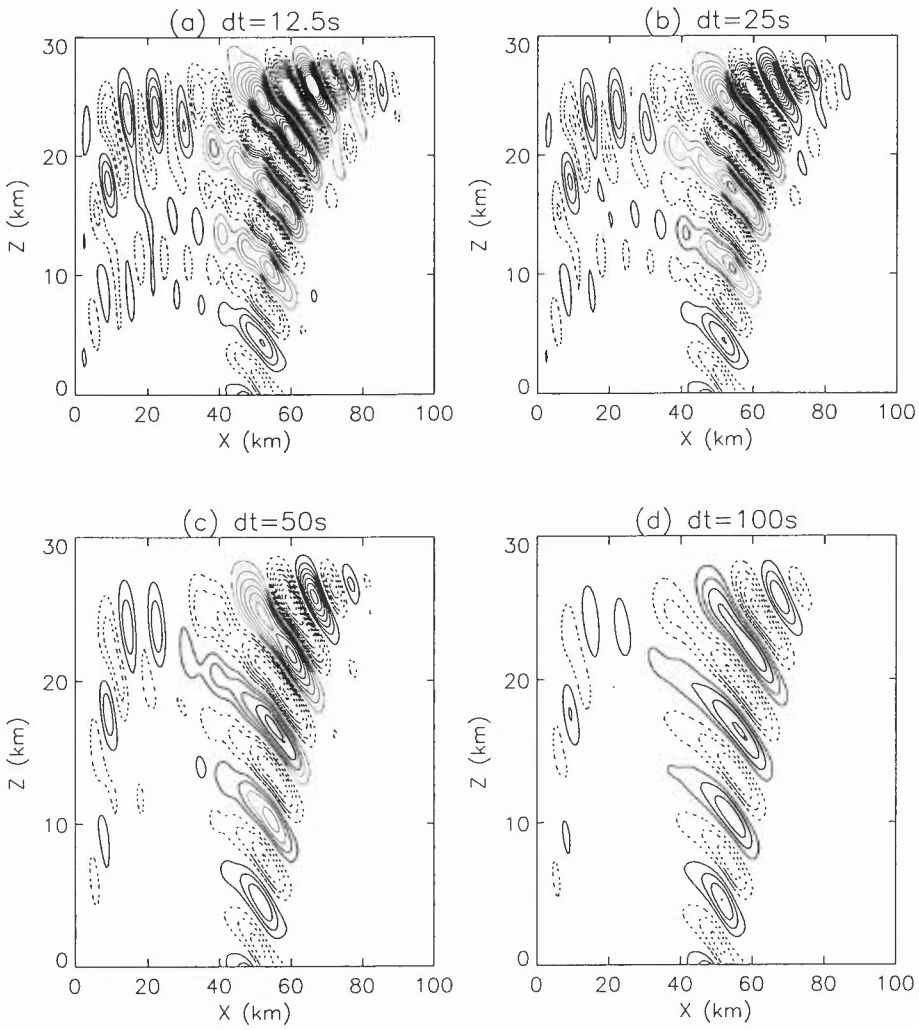


Figure 7: Vertical velocity field after 20,000s simulation: Effect of varying the timestep. The contour spacing is 0.025 m $s^{-1}$

Using a larger timestep has the effect of smoothing the wave field. However, a timestep of 100 seconds is still sufficient to resolve the low-level wave field, because an air parcel is advected a kilometre downwind during this time, which is only a tenth of the mountain length. However some of the magnitude is lost at altitudes around 10km. Using a smaller timestep results in a vertical velocity field which is noisier. This is counter-intuitive, as a smaller timestep should increase the accuracy of the simulation. It is possible that this noise is actually produced by the sponge layer, with smaller timesteps resulting in more interactions with the sponge for a given time. It was seen in figure (1) that introducing the sponge layer at the domain top created extra noise at the domain sides, which was then reduced using lateral sponges.

### 2.7 The Effect of Changing the Horizontal Resolution

Using a vertical resolution of 375m and a time-step of 50 seconds, the effect of varying the horizontal resolution was investigated. Figure (7) shows the vertical velocity fields after a 20000 second simulation for horizontal resolutions of 250m, 500m, 1km, 2km and 4km (Courant numbers of 2, 1, 0.5, 0.25 and 0.125), with a contour interval of 0.025 m $s^{-1}$.

Comparing these velocity fields and the values in table 1 with the linear analytical solution seen in figure (5), the best simulation results from a horizontal resolution of 1km or better. A grid spacing of 1km results in 20 grid-points across the mountain, which is sufficient for an accurate representation of the wave field. A larger grid spacing results in the loss of information and a reduction in wave amplitude, particularly for the 4km simulation for which there are less than 3 grid-points over the mountain. The smallest value of dx results in a wave amplitude which is 6% too large.

### 2.8 The Effect of Changing the Horizontal Domain Size

A final simulation was performed using a much larger domain length of 240km, with a horizontal resolution of 1km and a vertical resolution of 500m (adequate resolution to capture the wave field, but low enough to reduce the required computer time). A time-step of 50 seconds was used (Courant number of 0.5). The lateral sponge layers were widened to 70km to provide the strongest possible damping without affecting the actual wave field. Figure (8) shows the time development of the hydrostatic wave field for the central part of the domain, with contour levels 0.025 m $s^{-1}$. The times shown are 10000, 15000 and 20000 seconds, with figure (8d) showing the field at 20,000 seconds for the entire domain. The mountain is just fully grown after 10000 seconds, and the wave field is still in the developing stages, with small amplitudes and a limited vertical extent. After 15000 seconds, however, the wave field looks almost fully developed. There is only a small increase in the wave magnitude at lower levels in the next 5000 seconds. Virtually all the noise observed previously has now been eliminated and the simulation result is comparable to the linear analytical solution, although the magnitudes are under-predicted by 8% due to the combined effect of using horizontal and vertical resolutions of 1km and 500m respectively in an effort to reduce the computer time required.

## 3 Trapped Lee-waves

Keller (1994) demonstrated the differences between the results of a hydrostatic and a non-hydrostatic model for cases where non-hydrostatic effects become important in the presence of a vertical wind shear.

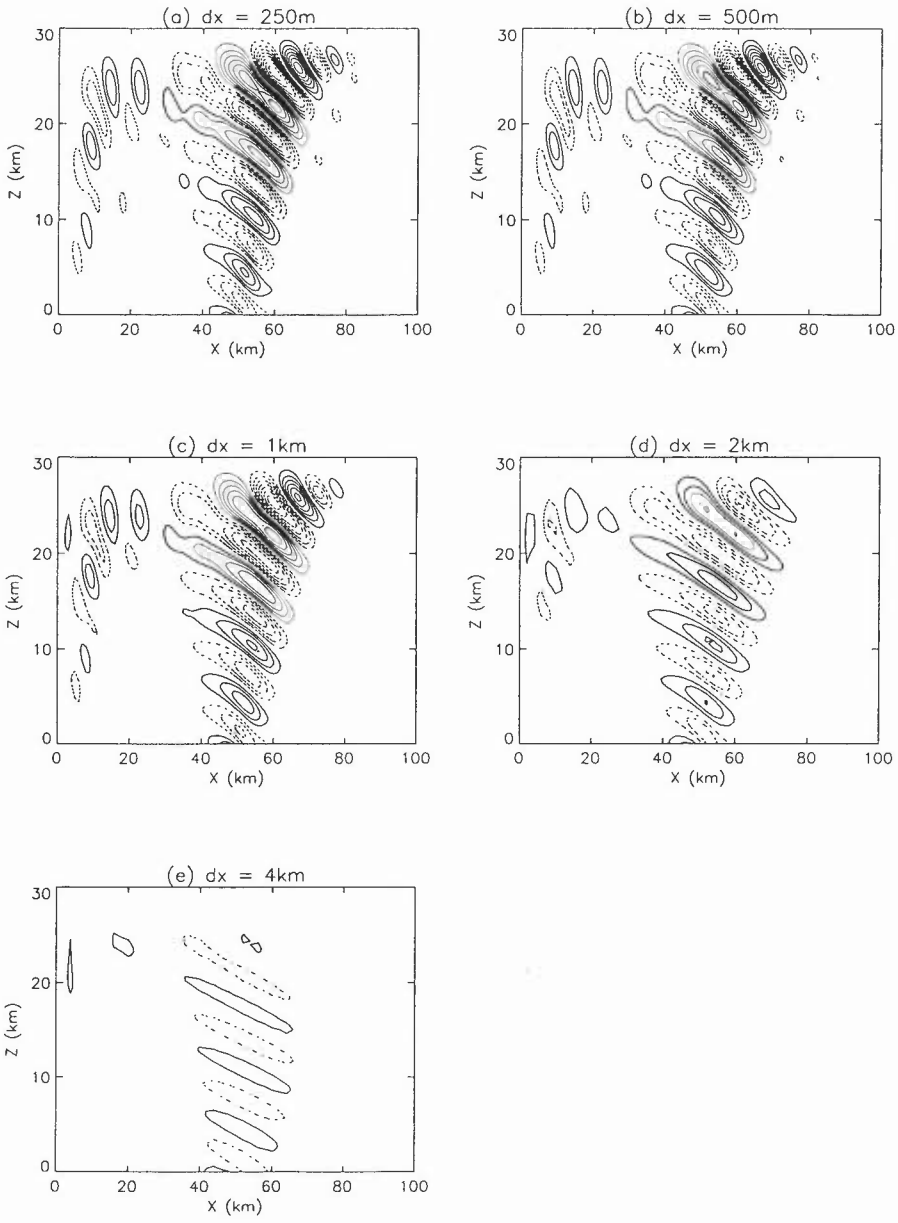


Figure 8: Vertical velocity field after 20,000s simulation: Effect of varying the horizontal resolution. The contour spacing is 0.025 m $s^{-1}$

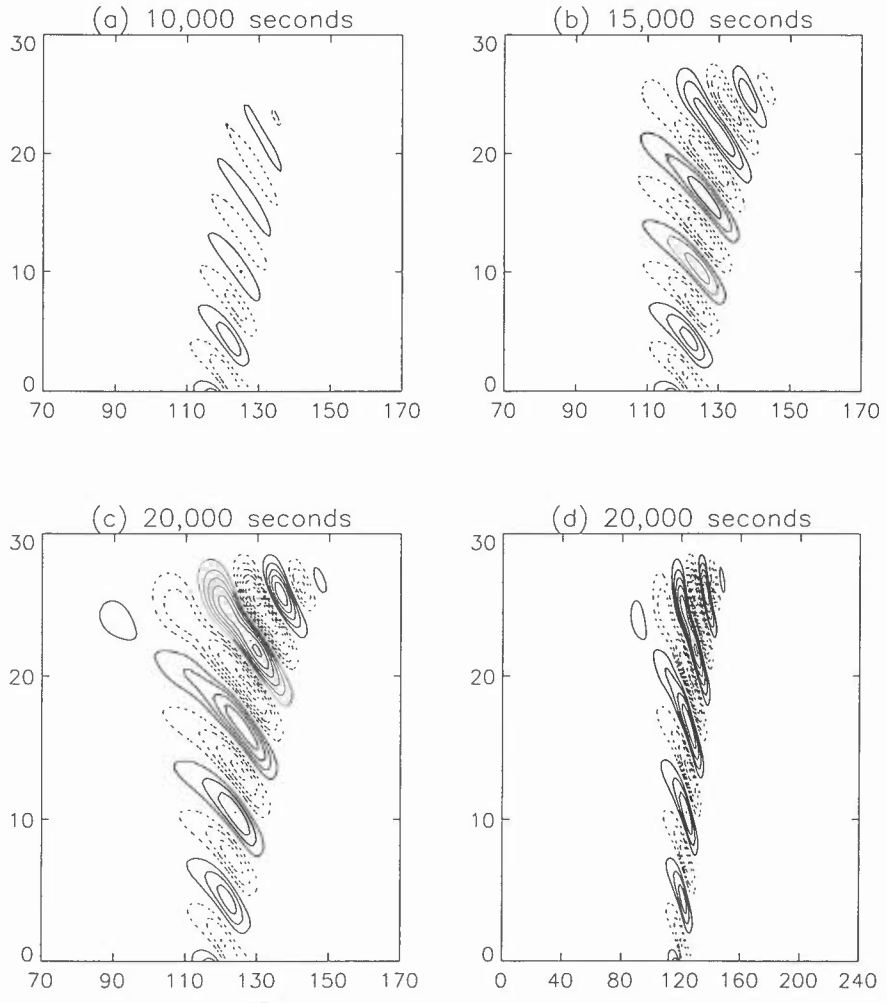


Figure 9: Time Development (a-c) of the vertical velocity field for the central part of a wider domain. The new domain width is 240km with lateral sponges of width 70km. Part (d) shows the final vertical velocity field for the entire domain. The contour spacing is 0.025 m $s^{-1}$

This is a common occurrence in the real atmosphere, where the wind speed often increases with height in the presence of an upper tropospheric jet. For such a positive wind shear, the Scorer parameter decreases with height to a very small value at the top of the domain. As the atmosphere will only support the vertical propagation of gravity waves with wavenumber k smaller than the Scorer parameter l, all waves forced at the lower boundary by flow over a mountain are trapped below some level determined by their wavelength. However, perfectly trapped waves are rare, as an increase in stability and reduction in wind-speed in the stratosphere often allows the waves to again propagate in the vertical, leading to the leakage of wave energy from the troposphere into the stratosphere (leaky lee-waves).

The fact that the New Dynamics model is non-hydrostatic means that we were able to simulate such trapped or leaky lee waves by introducing a wind-shear into the initial wind profile. For the case of perfectly trapped lee-waves (troposphere-only case), a constant value of N equal to 0.01 $s^{-1}$ was specified along with a wind profile defined as

$$U(Z) = U_0 + Z\frac{\delta U}{\delta z}$$

where $U_0$ is the surface wind-speed equal to 10 m $s^{-1}$, $\delta U/\delta z$ is the vertical wind shear equal to 0.0025 $s^{-1}$ and Z is the height in metres. For the troposphere-stratosphere case, a tropopause is introduced at a height of 10.5km above which the wind is constant at 36.25 m $s^{-1}$ (the value it reaches due to shear in the tropopause) and N is constant at 0.02 $s^{-1}$ (achieved using a step change at the tropopause). A Witch of Agnesi mountain profile was used with a half width of 2.5km and a maximum mountain height of 100m for the troposphere-only case and 500m for the troposphere-stratosphere case, as used by Keller (1994). The model domain was 150km long and 30km deep, with the mountain placed at a distance of 50km from the upwind boundary to allow for the development of lee-waves downstream of the mountain. The horizontal and vertical mesh lengths were both 500m.

Figure (9) shows the development of the vertical velocity wave field over 40000 seconds for the troposphere-only case with a time-step of 50 seconds (Courant number 1 at the surface). The contour interval is 0.04 m $s^{-1}$. A top-layer sponge is not required in such flows as the waves are not able to propagate vertically so that there are no reflections from the rigid lid. In fact, the result should be a standing wave trapped below a level determined by the Scorer parameter. Lateral sponges are not required either, as this would affect the wave field of interest. (In a test simulation with a horizontal domain of 250km with the mountain placed 100km downwind, the addition of 50km-wide lateral sponges made the resulting wave field worse, as did placing the mountain at the centre of the original domain). The resulting vertical velocity field shows two standing waves present with the shorter wave (larger wavenumber) trapped at lower levels. However, the magnitude is much smaller than that of Keller (1994), as indicated by the need to use a lower contour interval. Table 2 gives a wave magnitude of $\pm$ 0.44 m $s^{-1}$ after 40000 seconds.

Figure (10) shows the wave field development for the trapped lee-wave case with the time-step reduced to 12.5 seconds (surface CFL=0.25). The wave field is stronger for this lower time-step and reaches further downstream. Table 2 shows the wave magnitudes for the trapped lee-wave cases. The maximum wave magnitude reaches -0.65 and +0.51 m $s^{-1}$ after a 40000 second simulation with the smaller time-step. The model also predicts some upstream influence of the mountain on the airflow after 30000 seconds. With a smaller timestep, gravity and acoustic waves propagate faster in a semi-implicit scheme. This

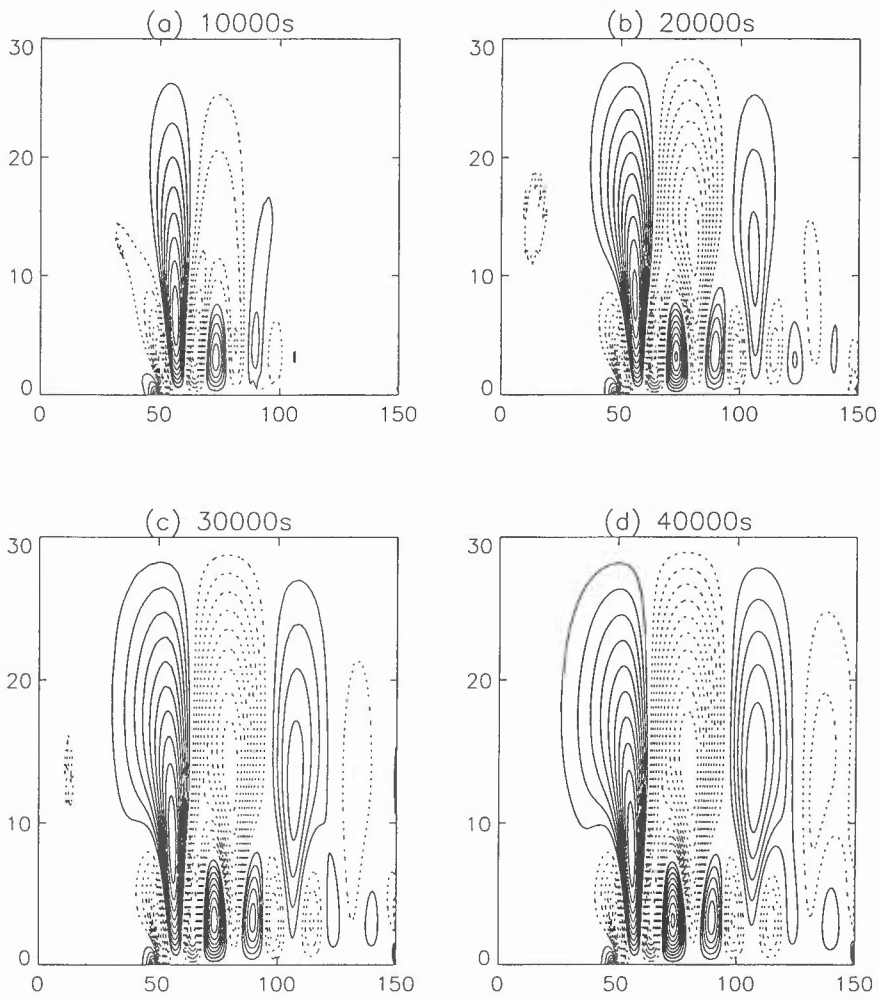


Figure 10: Trapped Lee-Waves: The time development of the vertical velocity field for the troposphere-only simulation, with 50s timestep. The contour spacing is 0.04 m $s^{-1}$

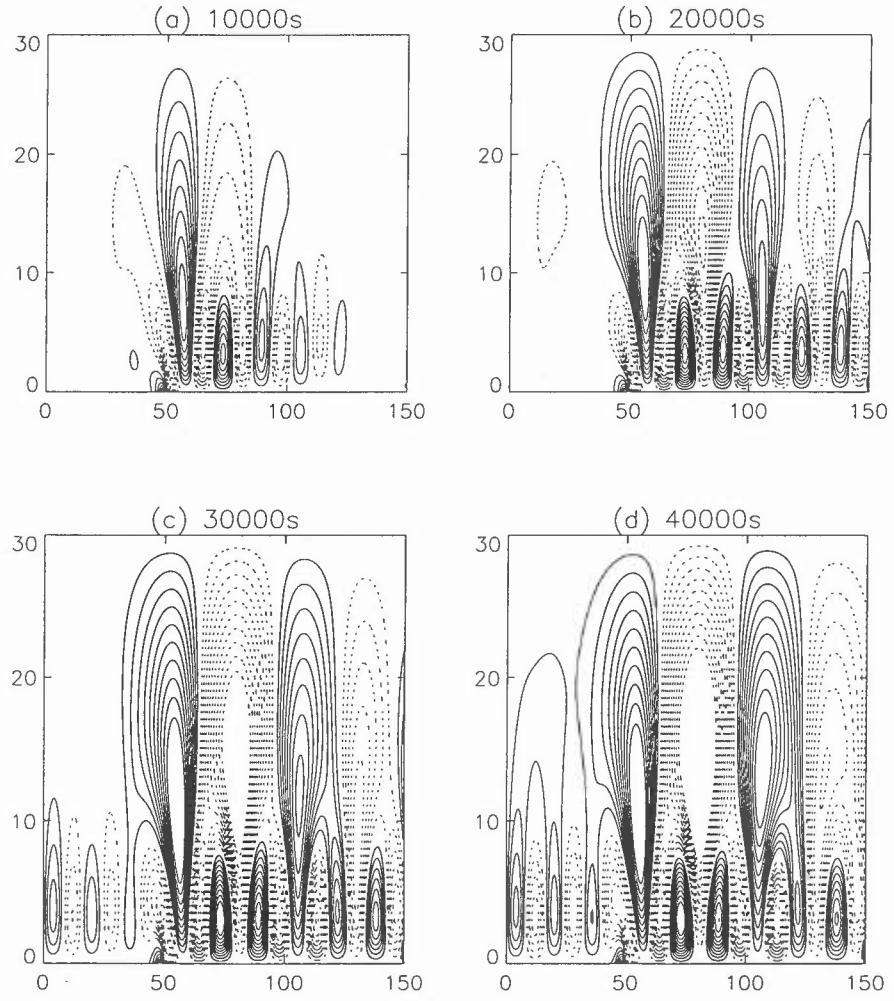


Figure 11: Trapped Lee-Waves: The time development of the vertical velocity field for the troposphere-only simulation with a smaller timestep of 12.5s. The contour spacing is 0.04 m $s^{-1}$

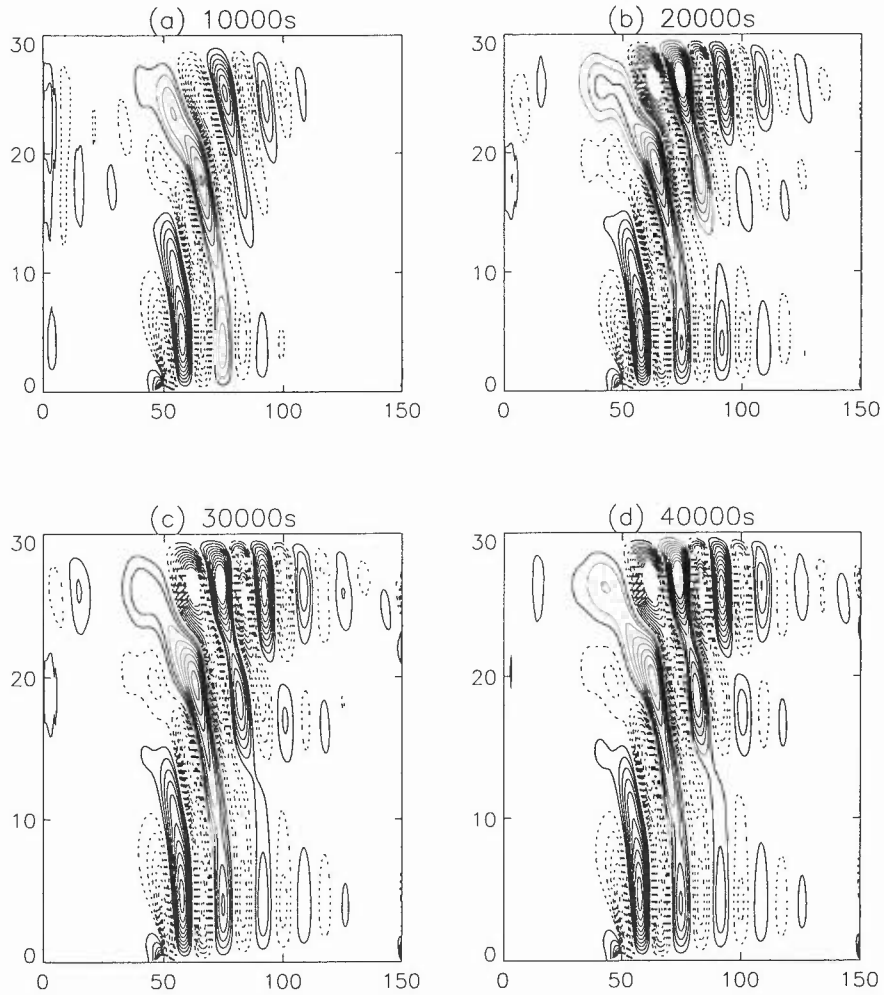


Figure 12: Leaky Lee-Waves: The time development of the vertical velocity field for a troposphere-stratosphere simulation with a 50s timestep. The contour spacing is 0.04 m $s^{-1}$

can be seen comparing figure 10 to figure 9 where the propagating trapped lee wave front can clearly be seen to be more advanced with a smaller timestep.

The New Dynamics uses a Semi-Lagrangian integration scheme which a stability analysis shows can be run stably (without spurious amplification of wave modes) at any Courant number. In this regard, the New Dynamics scheme is far less restrictive than traditional Eulerian finite difference schemes. However, in sheared flows semi-Lagrangian schemes have restrictions on the deformation Courant number ($\delta u/\delta x$ $\Delta$t) for the numerics to produce a physically realistic simulation. Experience from Eulerian schemes suggests that reducing the Courant number by reducing the timestep gives a smaller truncation error term and hence a more accurate numerical simulation. Reduction in the timestep also suppresses violation of the deformation Courant number criteria for 'physical' stability in a semi-Lagrangian scheme.

The introduction of a wind shear of 0.0025 m $s^{-1}$ results in a mean horizontal wind-speed of 35 m $s^{-1}$ at 10km, 60 m $s^{-1}$ at 20km and 85 m $s^{-1}$ at 30km. This means that at these higher levels the flow is advected a very large distance downstream in a 50 second time-step - a distance of 1.75km, 3km and 4.3km respectively. So at 20km the air is advected across a third of the mountain (which is 10km wide in this case). Within a time-step of 12.5 seconds, however, an air parcel at an altitude of 20km is only advected a distance of 750m. In other words, the air is advected across less than a tenth of the mountain.

The wave magnitude is much lower than that claimed by Keller even for the smaller time-step case. With Keller's specified contour interval of 0.2 m $s^{-1}$, the wave magnitude appears from figure 3 to be 1.6 m $s^{-1}$.

Figure (11) shows the result for the troposphere-stratosphere case with contour spacing of 0.2 m $s^{-1}$, as in Keller (1994). The waves are able to propagate again above the tropopause in this case and so a 15km deep sponge layer was used at the top boundary. The leaky lee-wave field is plagued by reflections from the top boundary, despite the use of the strongest sponge layer available in the code. The sponge is therefore unable to cope with such severe cases of wave reflection caused by the increased mountain height.

# 4 Conclusions

The results of a number of high resolution 2-dimensional simulations of stable flow over small mountains have been reported to investigate the performance of the New Dynamics. It has been shown that the model reproduces trapped lee-waves quite well in the presence of a constant vertical wind shear and constant stability. However, the presence of a stratosphere with higher stability and constant wind-speed above a height of 10.5km allowed the waves to propagate vertically, resulting in wave reflections from the rigid lid. These reflections were quite severe (due to using a 500m mountain) and the presence of the strongest available sponge layer was inefficient at reducing them.

For cases with constant upstream U and N, a hydrostatic gravity wave is simulated, with the propagation of wave energy vertically above the mountain. The vertical velocity field is contaminated by wave reflections from the rigid lid, but it was shown that the introduction of top and lateral sponge layers of sufficient depth and width respectively reduced these reflections to a manageable level if the run time is kept within reason (below about 20000 seconds for this case). However, they should not be so deep or so wide that they reduce the magnitude of the wave field itself. If wider lateral sponge layers are required, then a wider domain must be used. This has been shown to give better results, but requires more com-

puter time. The strongest sponge function available in the 2D code was chosen (a cosine squared function with $\alpha$ set to zero). The wave reflection problem should be less severe in the 3-dimensional version as the wave energy is also able to propagate horizontally.

However, problems with both the vertical and lateral sponge layers are evident. The introduction of these sponges could easily lead to the generation of unbalanced motions such as acoustic modes which could contaminate the flow field. An alternative approach which has been used successfully in numerical models is to smoothly degrade the vertical resolution. This reduces the accuracy of the numerical scheme making it more diffusive so that the wave energy propagating in the vertical is more effectively suppressed. This reduces the effect of significant wave reflection from the model upper boundary condition.

The results presented in this document show that model resolution and timestep must then be chosen carefully to give the best results for each case. As the New Dynamics uses a semi-Lagrangian integration scheme, there is no limit on the Courant number to retain numerical stability. However, there are other considerations for an accurate model run. Limitations on the deformation Courant number need to be respected to achieve a physically accurate simulation. The horizontal resolution should give at least 10 grid-points across the width of the mountain, while the vertical resolution should give at least 10 grid-points per vertical wavelength for hydrostatic waves. A small enough level spacing also eliminates the numerical noise which may be present in the lowest model layer.

The time-step must be chosen to limit the horizontal advection of any air parcel to a small fraction of the mountain width (about a tenth appears to be sufficient). This is easy for a constant upstream wind profile, but limits the time-step more severely when wind shear is present, as in the trapped lee-wave case. Too small a timestep, however, appears to cause problems within the sponge layer, producing small scale noise.

One problem with the use of the New Dynamics applied to idealized atmospheric conditions is to make sure that the initial conditions are consistent with the fluid equation set used. The use of an idealized exponential increase in potential temperature leads to the atmospheric pressure becoming zero somewhere between 30 and 40km (depending on the choice of tropospheric and stratospheric Brunt-Vaisala frequencies). If a more realistic choice of atmospheric profile is chosen the atmospheric pressure will still be positive at large heights. What is clear, however, is that the non-hydrostatic formulation of the new dynamics makes it ideal for studying typical atmospheric wave fields. Care is needed in chosing model domain, resolution and timestep for particular cases. Care is also needed in dealing with wave energy propagation towards lateral boundaries and the top of the model to restrict the problem of unwanted wave reflections.

# 5 References

T. L. Keller (1994). Implications of the hydrostatic assumption on atmospheric gravity waves. *J. Atmos. Sci.*, **51**, 1915–1929.

J. B. Klemp and D. K. Lilly (1978). Numerical simulation of hydrostatic mountain waves. *J. Atmos. Sci.*, **35**, 78–107.

R. B. Smith (1979). The influence of mountains on the atmosphere. *Adv. Geophys.*, **21**, Academic

Press, 87–230.

# 6 Acknowledgements

Thanks to Drs. A. Staniforth and N. Wood (NWP) for their thorough appraisal and constructive comments on this document.

**Table 1** Minimum and maximum vertical velocity values for the hydrostatic gravity wave case over the entire model domain and in the lowest 10km for all figures shown.

| Figure | Min W | Max W | Min below 10km | Max below 10km |
|---|---|---|---|---|
| 1a | -0.386 | 0.420 | -0.086 | 0.088 |
| 1b | -0.309 | 0.325 | -0.086 | 0.087 |
| 1c | -0.150 | 0.144 | -0.084 | 0.088 |
| 1d | -0.157 | 0.149 | -0.085 | 0.088 |
| 1e | -0.500 | 0.760 | -0.088 | 0.103 |
| 1f | -0.476 | 0.696 | -0.085 | 0.094 |
| 1g | -0.396 | 0.510 | -0.095 | 0.092 |
| 1h | -0.322 | 0.224 | -0.094 | 0.099 |
| 2a | -0.202 | 0.158 | -0.084 | 0.089 |
| 2b | -0.157 | 0.149 | -0.085 | 0.088 |
| 2c | -0.123 | 0.120 | -0.084 | 0.088 |
| 3 | -0.160 | 0.146 | -0.086 | 0.092 |
| 4a | -0.160 | 0.146 | -0.086 | 0.092 |
| 4b | -0.201 | 0.175 | -0.099 | 0.099 |
| 4c | -0.218 | 0.185 | -0.104 | 0.109 |
| 6a | -0.208 | 0.275 | -0.112 | 0.127 |
| 6b | -0.184 | 0.239 | -0.109 | 0.120 |
| 6c | -0.154 | 0.185 | -0.104 | 0.109 |
| 6d | -0.111 | 0.122 | -0.094 | 0.101 |
| 7a | -0.221 | 0.189 | -0.107 | 0.109 |
| 7b | -0.218 | 0.186 | -0.104 | 0.109 |
| 7c | -0.190 | 0.166 | -0.097 | 0.101 |
| 7d | -0.097 | 0.103 | -0.077 | 0.078 |
| 7e | -0.050 | 0.045 | -0.050 | 0.045 |
| 8a | -0.074 | 0.067 | -0.074 | 0.067 |
| 8b | -0.095 | 0.098 | -0.086 | 0.088 |
| 8c | -0.180 | 0.157 | -0.092 | 0.093 |
| 8d | -0.180 | 0.157 | -0.092 | 0.093 |

**Table 2** Minimum and maximum vertical velocity values for the trapped leewave (troposphere only) case over the entire domain, using 50s (figure 9) and 12.5s (figure 10) timesteps.

| Figure | Min W | Max W |
|---|---|---|
| 9a | -0.286 | 0.351 |
| 9b | -0.325 | 0.415 |
| 9c | -0.391 | 0.432 |
| 9d | -0.445 | 0.432 |
| 10a | -0.307 | 0.358 |
| 10b | -0.413 | 0.456 |
| 10c | -0.552 | 0.566 |
| 10d | -0.649 | 0.508 |

**Table 3** Minimum and maximum vertical velocity values for the leaky leewave (troposphere-stratosphere) case over the entire model domain and in the lowest 8km.

| Figure | Min W | Max W | Min below 8km | Max below 8km |
|---|---|---|---|---|
| 11a | -1.862 | 1.802 | -1.591 | 1.802 |
| 11b | -2.595 | 2.532 | -1.568 | 2.167 |
| 11c | -2.563 | 2.504 | -1.564 | 2.121 |
| 11d | -2.648 | 2.498 | -1.581 | 2.125 |